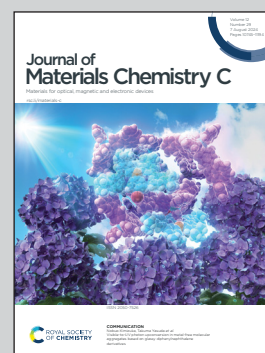**Showcasing research from Professor Svoboda's laboratory, Department of Organic Chemistry, University of Chemistry and Technology, Prague, Czech Republic.**

Competing synclinic and anticlinic interactions in smectic phases of bent-core mesogens

Presented liquid crystalline molecules combine two features, the bent-core rigidity with the dimeric character, and they reveal variety of specific phases depending on the length of alkyl spacer. Longer homologues exhibit a predisposition towards the formation of tilted smectic phases, which are characterized by complex sequences of synclinic and anticlinic interfaces. Conversely, shorter homologues demonstrate a propensity for helical smectic structures. For intermediate homologues, the frustration is alleviated through the formation of several modulated smectic phases.

ROYAL SOCIETY
OF **CHEMISTRY**

rsc.li/materials-c

Registered charity number: 207890

Check for updates

Competing synclinic and anticlinic interactions in smectic phases of bent-core mesogens†

Jiří Svoboda, [ID] [a] Václav Kozmík,[a] Kvetoslava Bajzíková,[a] Michal Kohout, [ID] [a] Vladimíra Novotná, [ID] *[b] Natalia Podoliak, [ID] [b] Damian Pociecha [ID] [c] and Ewa Gorecka [ID] [c]

Recent studies on liquid crystals (LCs) have focused on structurally new molecular systems forming phases distinct from simple nematic or smectic ones. Sophisticated molecular shapes may reveal structural complexity, combining helicity and polarity. Mirror symmetry-breaking in bent-core molecules can lead to a propensity for synclinic and anticlinic molecular structures within consecutive smectic layers. On the other hand, despite their achiral character, dimers readily adopt helical phases. In this study, we investigate a hybrid molecular structure incorporating both characteristics, namely a rigid bent-core and an attached bulky polar group *via* a flexible spacer. To perform phase identification, we enrich standard experimental methods with sophisticated resonant soft X-ray scattering technique. Notably, we observe a distinct preference for specific phase types depending on the length of the homologue. Longer homologues exhibit a predisposition towards the formation of tilted smectic phases, which are characterized by complex sequences of synclinic and anticlinic interfaces. Conversely, shorter homologues demonstrate a propensity for helical smectic structures. For intermediate homologues, the frustration is alleviated through the formation of several modulated smectic phases. On the basis of the presented study, we describe the preconditions for high-level structures in relation to conflicting constraints.

1. Introduction

Over the years, two categories of thermotropic liquid crystals (LCs) have captured attention: those composed of rod-like molecules that form nematic and smectic phases and disc-like molecules that prefer columnar phases.[1] In the past years, the focus has shifted to less conventional mesogenic structures, and the group that has become particularly intriguing comprises molecules with a bent shape.[2–9] These molecules are either dimers, composed of two mesogenic parts connected with a flexible spacer with an odd number of atoms,[10–14] or they have an extended rigid core with usually a central *meta*-substituted phenyl or naphthalene ring.[15–23] A rigid bent-core structure restricts molecular rotation, which in turn might induce correlations of dipoles. Bent dimers also facilitate low bend elasticity,[24,25] which leads to a heliconical molecular

arrangement.[26] Consequently, rigid bent-core mesogens have a strong tendency to form polar phases,[14–16] and flexible dimers readily form helical phases.[27] In this study, our focus is on the molecules that combine both characteristics. The studied compounds feature a large rigid core typical for bent-core molecules, extended in one arm *via* a flexible alkoxy linker, which is terminated by a bulky nitrophenyl moiety.

In our previous work,[28] we studied the effect of various terminal groups (phenylalkyl, phenyloxyalkyl, thienylalkyl, and substituted phenylalkoxy) on the mesomorphic properties of a series of naphthalene-based bent-core molecules. For these compounds, we detected the nematic and columnar phase.[28] Additionally, for the longer homologues with extended connecting parts, a dark-conglomerate phase has been observed, evidencing chiral symmetry breaking.[29] For the materials presented here, we extended the molecular arm and modified the polarity of the terminal group in comparison with the previously introduced molecular structures[30–32] to enhance dipolar interactions. Nowadays, the terminal nitro group, which introduces large longitudinal dipole moment has stimulated intensive research after the discovery of a ferroelectric nematic phase.[33,34] We aim to shed light on the modification of self-assembly processes in bent core molecules with such a bulky polar terminal group attached to a flexible spacer.

[a] Department of Organic Chemistry, University of Chemistry and Technology, CZ-166 28 Prague 6, Czech Republic

[b] Institute of Physics of the Czech Academy of Sciences, Na Slovance 2, CZ-182 21 Prague 8, Czech Republic. E-mail: novotna@fzu.cz

[c] Faculty of Chemistry, University of Warsaw, ul. Zwirki i Wigury 101, 02-089 Warsaw, Poland

† Electronic supplementary information (ESI) available. See DOI: https://doi.org/10.1039/d4tc01695e

This journal is © The Royal Society of Chemistry 2024

J. Mater. Chem. C, 2024, **12**, 10903–10909 | **10903**

2. Results and discussion

A series of mesogens with molecules having a rigid naphthalene-based bent core, terminated on one side with a dodecyloxy chain, is synthesized (Fig. 1). A nitro-substituted phenyl ring is attached to the core *via* a flexible alkoxy linker on the other side. The homologues are denoted as **I-*n***, where *n* represents the number of carbon atoms in the spacer, ranging from 4 to 12. The synthesis procedures are described in ESI.† Except for the materials with the shortest alkyl chain (**I-4** and **I-5**), all compounds exhibit a nematic phase (N) below the isotropic liquid (Iso), which is followed by a smectic A (SmA) phase on cooling. Contrary to the behavior of typical rod-like mesogens, for which elongated terminal chains destabilize the nematic phase in favor of the smectic phases in the studied homologue series, the nematic phase temperature range expands with the elongation of the alkoxy spacer group. Most probably, when the lengths of alkyl chains attached to both arms of the mesogenic cores become comparable, the interactions between the mesogenic cores and the nitrophenyl terminal groups increase, which reduces the tendency to form layers.

The phase transition temperatures and their corresponding enthalpies obtained from the DSC measurements are presented in Table 1 and the final phase diagram is presented in Fig. 2. Most phase transitions were clearly distinguishable during the DSC measurements. The only exception is the SmC_1–SmC_2 phase transitions, which were detected based on the textural changes and birefringence measurements. Except for the SmC_{TB} phase in homologue **I-8** and the SmC_2–SmC_2'–SmC_1'' phase sequence in homologue **I-9**, the observed mesophases are detected on the heating and cooling runs, exhibiting an enantiotropic character. The clearing and the N-SmA phase transition temperatures exhibit a general decrease with the elongation of the molecules, and an odd–even effect is superimposed on this trend, which is especially pronounced for short homologues. Molecules with a spacer built of an even number of atoms display higher transition temperatures, which is attributed to a more efficient packing in the case when the terminal nitrophenyl group is aligned parallel to the mesogenic arm of the molecule. Let us point out that the transition enthalpy values for the N-SmA show an odd–even effect opposite that observed for the transition temperatures, *i.e.* there is a larger enthalpy for odd homologues.

A phase diagram of series **I-*n*** (Fig. 2) essentially splits into two distinct regions, with homologue *n* = 9 exhibiting a crossover behavior. For homologues with *n* < 9, tilted phases, either anticlinic or heliconical (of the SmC_{TB} type), are formed below

the SmA phase. However, for homologues with *n* > 9, non-helical tilted smectic phases are observed, displaying a complex tilt structure. This discrimination is also evident when analyzing the temperature dependence of the layer spacing, *d*, in the smectic phases (Fig. 3). Short homologues exhibit the positive thermal expansion of the layer thickness in the whole temperature range and a very strong odd–even effect – layer spacing is systematically larger for even homologues than for the neighboring odd ones. In contrast, longer homologues in lower temperature phases display negative thermal expansion of the layer thickness, and the parity of the spacer has a much weaker effect on the *d* value.

2.1. Mesomorphic properties of the short homologues

In this subsection, we describe the behavior of the short homologues, with *n* < 9. Below the Iso and N phases, the SmA phase appeared. The SmA phase is optically uniaxial, and in cells with homeotropic anchoring (HT), a uniform black texture without any recognizable features is observed. Upon cooling to the phase below the SmA phase, a schlieren-like texture emerges (Fig. S2, ESI†), which could suggest either a SmA_b (biaxial non-tilted smectic phase, in which molecules show restricted rotation along the long axis) or a tilted smectic phase. Doping of the studied material with a small amount (less than 1%) of chiral additive makes the phase optically uniaxial. Such a small concentration of the chiral dopant does not make changes in the mesophase range, and only the symmetry changes upon chiral admixture. For details about the chiral molecules, see ESI.† This type of experiment allows for the identification of a tilted, SmC-type, phase.

For homologues **I-7** and **I-8**, another SmC phase is observed on further cooling, with uniaxial optical properties (appearing dark in the case of homeotropic anchoring when placed between crossed polarizers, see Fig. S3, ESI†). The X-ray diffraction studies revealed the layer spacing corresponding to a single molecular length in all smectic phases, slightly decreasing on cooling, with no anomalies observed at the phase transitions. No layer spacing change suggests that both tilted phases have nearly the same tilt magnitude, and the optical uniaxial properties of the lower tilted phase point have a helical SmC_{TB}-type structure.

In a cell with planar anchoring conditions (HG cell), the light extinction direction remains along the rubbing direction in all smectic phases. This indicates an anticlinic structure of the upper temperature tilted phase – SmC_A phase. The temperature dependence of optical birefringence (Δn) is consistent with a continuous increase in molecular tilt below the SmA phase (Fig. 4). In the tilted smectic phases, the birefringence begins to decrease from the value extrapolated from the critical dependence found in the nematic and smectic A phases. The SmC_A–SmC_{TB} phase transition is marked with a slight, step-like increase in Δn, and a further deviation from the extrapolated value is observed during cooling. Interestingly, in HT cells, careful microscopic observations at the SmC_{TB} to SmC_A phase transition revealed a selective light reflection phenomenon (Fig. 4). In ~1 K temperature range at this phase transition,
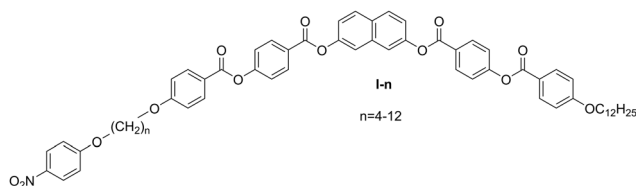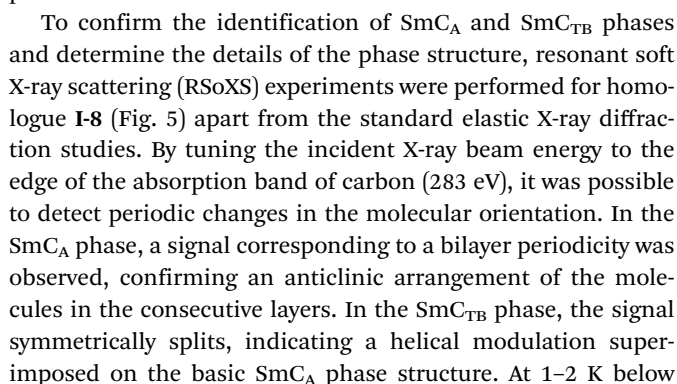

Fig. 1 General chemical formula of the studied compounds.

I-*n*

n=4-12

10904 | *J. Mater. Chem. C*, 2024, **12**, 10903–10909

This journal is © The Royal Society of Chemistry 2024

Table 1 DSC measurements results: the melting points, m.p., taken on the second heating, the phase transition temperatures, T_{tr}, and the crystallization temperature, T_{cr}, subsequently measured on the second cooling from the isotropic phase, are in °C, and corresponding enthalpy changes, ΔH (kJ mol^{-1}) in brackets at the corresponding temperature. The symbol * indicates that the temperature was established from X-ray measurements as corresponding peaks were not detectable during DSC measurements

	M.p. [ΔH]	T_{cr} [ΔH]	T_{tr} [ΔH]	T_{tr} [ΔH]	T_{tr} [ΔH]	T_{tr} [ΔH]	T_A [ΔH]	T_{iso} [ΔH]
I-4	148 [+30.5]	128 [−30.6]				SmC$_A$ 164 [−0.89]	SmA 198 [−2.7]	—
I-5	130 [+20.0]	102 [−27.1]				SmC$_A$ 156 [−0.60]	SmA 167 [−2.5]	—
I-6	121 [+22.5]	98 [−21.1]				SmC$_A$ 153 [−0.17]	SmA 181 [−0.79]	184 [−0.99]
I-7	113 [+23.5]	88 [−18.9]	SmC$_{TB}$ 132 [−0.03]			SmC$_A$ 146 [−0.04]	SmA 162 [−1.16]	N 165 [−0.31]
I-8	130 [+54.7]	105 [−46.8]	SmC$_{TB}$ 118 [−0.01]			SmC$_A$ 140 [−1.25]	SmA 168 [−0.50]	N 173 [−0.67]
I-9	127 [+45.4]	93 [−19.5]	SmC$_2'$ 116 [−0.14]	SmC$_2'$ 118 [*]		SmC$_1'$ 135 [−0.25]	SmA 158 [−2.7]	N 162 [−0.51]
I-10	122 [+36.1]	100 [−25.9]	SmC$_2$ 123 [*]	SmC$_1''$ 122 [−0.35]	SmC$_1$ 136 [*]	SmC$_1$ 131 [−0.51]	SmA 159 [−0.72]	N 166 [−0.36]
I-11	131 [+27.1]	109 [−21.7]	SmC$_2$ 142 [*]			SmC$_1$ 143 [−2.63]	SmA 153 [−1.46]	N 158 [−0.63]
I-12	129 [+35.2]	98 [−31.7]	SmC$_2$ 142 [−3.01]				SmA 151 [−0.55]	N 159 [−1.08]

Fig. 2 Phase diagram of the studied homologues upon elongation of the spacer between the rigid core and the terminal nitrophenyl group. Gray tiled area shows the stability range of the crystal phase marked by melting points.

colors change from blue to red with increasing temperature, providing evidence of the helix unwinding. It is worth noting that the helix unwinding found in this material is very similar to the phenomena observed for dimers at the SmC$_{TB-SH}$–SmC$_{TB-DH}$ phase transition.[14]

To confirm the identification of SmC$_A$ and SmC$_{TB}$ phases and determine the details of the phase structure, resonant soft X-ray scattering (RSoXS) experiments were performed for homologue **I-8** (Fig. 5) apart from the standard elastic X-ray diffraction studies. By tuning the incident X-ray beam energy to the edge of the absorption band of carbon (283 eV), it was possible to detect periodic changes in the molecular orientation. In the SmC$_A$ phase, a signal corresponding to a bilayer periodicity was observed, confirming an anticlinic arrangement of the molecules in the consecutive layers. In the SmC$_{TB}$ phase, the signal symmetrically splits, indicating a helical modulation superimposed on the basic SmC$_A$ phase structure. At 1–2 K below

Fig. 3 Smectic layer thickness, d, measured as a function of temperature for the studied homologues **I-n**. In the inset, the layer spacing in the SmA phase, determined 5 K below the Iso-SmA or N-SmA phase transition (dashed line on the main panel), is presented.

This journal is © The Royal Society of Chemistry 2024

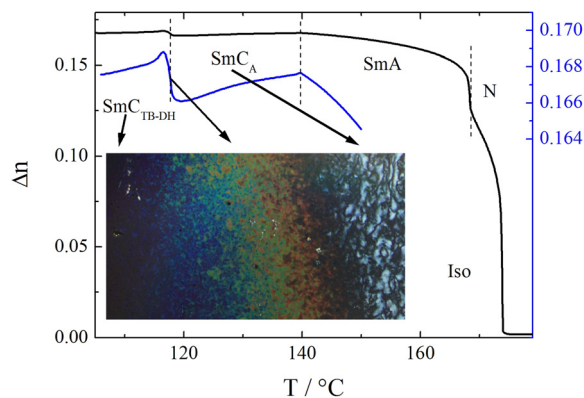J. Mater. Chem. C, 2024, **12**, 10903–10909 | **10905**

Fig. 4 Temperature dependence of optical birefringence, Δn (black line), for the homologue **I-8** measured with green light, $\lambda = 532$ nm. A blue line presents a fragment of zoomed $\Delta n(T)$ dependence (see the right axis). In the inset, the texture observed in the HT cell with a temperature gradient is presented. In a small temperature range ($\sim$1 K) near the SmC$_A$–SmC$_{TB-DH}$ phase transition, the colors are observed due to the selective reflection of light from the helical structure formed in the SmC$_{TB-DH}$ phase. The colors change in sequence from blue to red as the temperature increases.
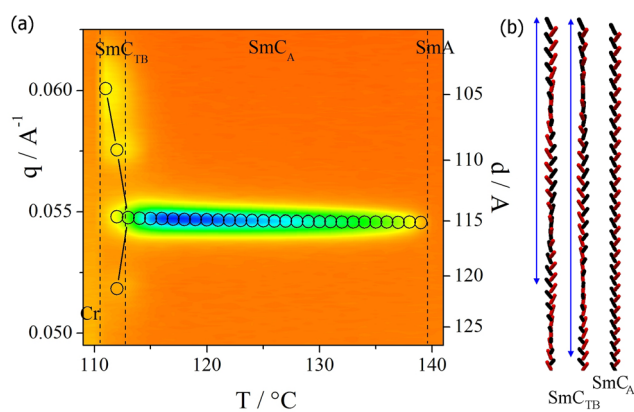

Fig. 5 (a) Temperature evolution of RSoXS signals for **I-8**. In the SmC$_A$ phase, the position of the signal corresponds to 2 molecular layers, and the splitting of the signal in the SmC$_{TB-DH}$ phase is caused by the additional modulation of molecular orientation as the helix is superimposed on the SmC$_A$ bilayer structure. (b) Model of the anticlinic and the helical structures of SmC$_A$ and SmC$_{TB-DH}$ phases, respectively; the structures with two different helical pitch lengths (marked by blue arrows) are schematically illustrated.

the SmC$_A$–SmC$_{TB}$ phase transition, the helical pitch, estimated from the distance of the split signals in q-space, is $\sim$200 nm ($\sim$30 smectic layers). Unfortunately, the crystallization of the sample precluded a more precise determination of the temperature evolution of the pitch length by the resonant X-ray studies. Schematic models of the anticlinic and the helical structures of SmC$_A$ and Sm$_{CTB-DH}$ phases with two different helical pitch lengths are presented in Fig. 5; for details, see Abberley *et al.*[27] However, the combination of the resonant X-ray and optical studies, in which the selective light reflection from the helix is found in a visible optical range, clearly points to the critical unwinding of the helix upon entering the anticlinic SmC$_A$ phase.
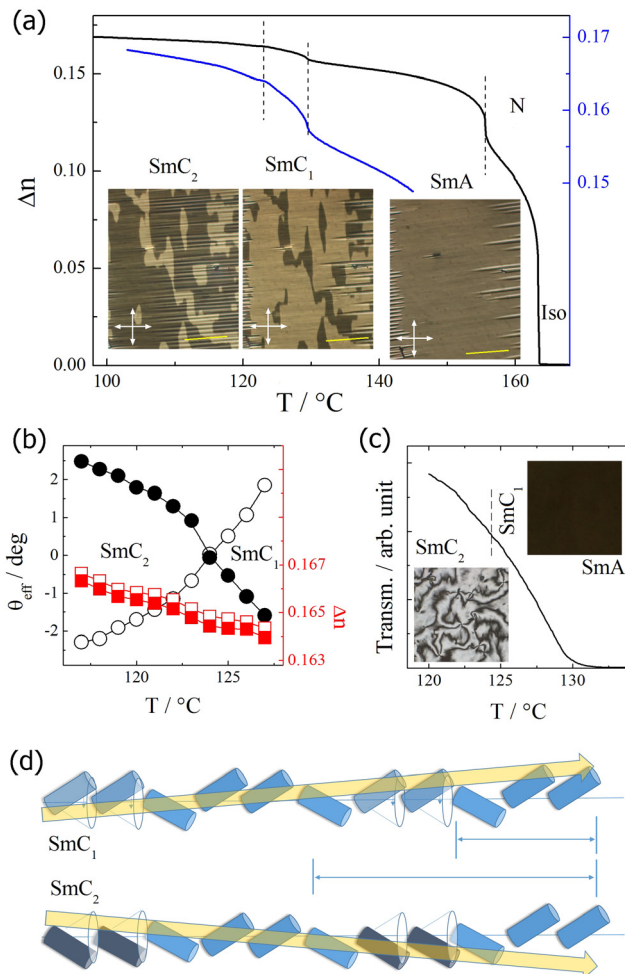

Fig. 6 (a) Temperature dependence of optical birefringence, and Δn (black line) for homologue **I-10** (blue line presents a fragment of the zoomed $\Delta n(T)$ dependence, see the right axis). In the inset, the textures of SmA and tilted SmC$_1$ and SmC$_2$ phases, the brightness of tilt domains in the SmC phases, is interchanged as the tilt inversion occurs at the SmC$_1$–SmC$_2$ phase transition. Arrows represent polarizer directions, and yellow lines indicate rubbing direction, which is slightly inclined from the polarizer direction. (b) Temperature dependence of the apparent tilt angle (θ_{eff}) in the two types of domains (open and solid black circles) and the optical birefringence (red squares) measured in μm-size spots in the domains across the SmC$_1$–SmC$_2$ phase transition. (c) Light transmission through the HT cell; the inversion of the apparent tilt at the SmC$_1$–SmC$_2$ phase transition is not connected with any light transmission anomaly; thus, any in-plane birefringence changes. In the inset photographs, the texture in the same area of the sample is shown in the SmA and SmC$_2$ phases. (d) Model of the tilt arrangement in the consecutive smectic layers in the SmC$_1$ and SmC$_2$ phases; a 3-layer repeating unit (upper blue arrow) of the SmC$_1$ changes to a 6-layer unit (lower blue arrow) in the SmC$_2$ phase *via* molecular rotation on the tilt cone in the marked layers, which results in the inversion of the apparent optical tilt direction (yellow arrows).

2.2. Mesomorphic properties of the long homologues

For homologues with $n > 9$, two smectic phases, SmC$_1$ and SmC$_2$, were found upon cooling below the SmA phase (Fig. 2). The XRD studies revealed a layer spacing corresponding to a single molecular length and a liquid-like in-plane ordering of the molecules in these phases. A small step-like increase in the

10906 | *J. Mater. Chem. C*, 2024, **12**, 10903–10909

This journal is © The Royal Society of Chemistry 2024

layer thickness was observed at the transition SmC_1–SmC_2. Moreover, the lower-temperature phase exhibited a negative thermal expansion coefficient.

In HG cells, the SmA phase showed a uniform texture with the extinction direction along the rubbing direction, which is covered with a regular array of strongly elongated focal conics. A regular array of stripes was observed in thin HG cells, similar as it was reported for twist-bend (TB) phases.[34–37] Upon cooling, in the stripe-free regions, several micron-sized domains are formed at the transition to the SmC_1 phase; with the extinction direction inclined from the rubbing direction by a few degrees, the domains can be brought into light extinction conditions by rotating the sample either clockwise or anticlockwise (Fig. 6a). Such a texture unequivocally indicates a tilted smectic phase. Interestingly, at the SmC_1–SmC_2 phase transition, the tilt direction reverses within each domain without affecting the domain boundaries; the change in the apparent tilt angle is continuous (Fig. 6b). This phenomenon occurs without pronounced changes in the birefringence of the sample (Fig. 6a), and it is reversible upon heating and cooling. To confirm that this effect is inherent to the material and not induced by surface interactions, samples of various thicknesses were tested, and the tilt direction inversion was consistently reproduced in all of them.

In the HT cell, both tilted smectic phases exhibit a schlieren texture, confirming their optical biaxial character (Fig. 6c). The in-plane birefringence (and, thus, the optical texture) shows no anomaly at the SmC_1–SmC_2 phase transition, which suggests that a change in the tilt magnitude does not accompany the transition. Apparently, none of the tilted phases are simple synclinic (S) or anticlinic (A) type, and both have a complex sequence of S and A interlayer interfaces. The exact mechanism behind the SmC_1–SmC_2 phase transition needs to be elucidated, but it surely involves the change in order and number of synclinic and anticlinic interfaces. One of the simplest possibilities involves doubling the basic multilayer repeating unit on the transition from the SmC_2 to SmC_1 phase, with the sequence of interlayer interfaces changing from a 3-layer SAA unit to a 6-layer SASSSA unit (Fig. 6d). When observed in planar cell geometry, such a change results in the inversion of the effective/apparent optical tilt direction without affecting its magnitude in single layers.

2.3. Mesomorphic properties of the homologue I-9

The homologue with $n = 9$ displays the most complex phase sequence, featuring five tilted smectic phases below the SmA phase, which all are characterized by a liquid-like in-plane order of the molecules. Each smectic-smectic phase transition is accompanied by a small step-like anomaly in the optical birefringence (Fig. 7). The optical textures of all the phases observed in HG cells resembled those observed for longer homologues, and the inversion of the apparent tilt angle in tilted domains was found (Fig. S4, ESI†). We decided to label the phases as SmC_1', SmC_1, SmC_1'', SmC_2', and SmC_2 subsequently on cooling from the SmA phase. The inversion phenomenon occurs at the transition between the SmC_1'' and
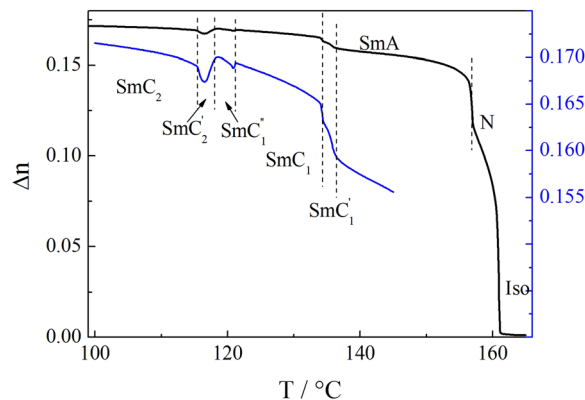

Fig. 7 Temperature dependence of the optical birefringence for **I-9**. Blue curve presents this dependence in an enlarged view (see the right scale).

SmC_2' in the analogous way described for the homologues with $n > 9$.

The transitions between the smectic phases are not accompanied by a significant change in textures observed in planar geometry. In HT cells, however, the phase transitions are accompanied by changes in optical textures (Fig. S5, ESI†), and some of the observed textures indicate the formation of 2D-modulated phases. Below the optically uniaxial SmA phase, a weakly birefringent fan-like texture is formed, and only the lowest SmC_2 phase is characterized by a simple schlieren texture, which is typical for a simple lamellar-tilted smectic phase. Similar to longer homologues, there are no texture changes during the transition between the SmC_1 and SmC_2 phases, at which the inversion of the apparent tilt occurs.

X-ray diffraction studies revealed that in all the smectic phases, the main periodicity related to the density modulation along the layer normal (indicated by the strongest diffraction signal) closely matches the molecular length. However, in all the phases except for the SmA and the lowest temperature SmC_2, additional weak signals associated with a bilayer structure are detected (Fig. 8a). This finding suggests the breaking of the up-down equality in the molecular arrangement within the layers possibly due to the interactions between strongly polar nitrophenyl end-groups and the formation of 'weak dimeric' units. In none of those phases, the positions of the additional signals commensurate with the diffraction signals coming from the layer thickness, signifying that the electron density is modulated along the smectic layers, and 2D-modulated structures are formed, all having oblique crystallographic unit cells (Fig. S6, ESI†). The determined in-plane modulation period changes in consecutive phases, and it is very long, 200–300 Å, in all cases. Moreover, the inclination angle of the crystallographic unit cell is different in each modulated phase and not consistent with the tilt found by optical methods in these phases. Therefore, we conclude that the in-plane density modulations grow independently of the tilt structure, and the density waves defining a 2D crystallographic structure develop in the direction perpendicular to the tilt plane (Fig. 8b).

We studied dielectric spectroscopy in a broad range of frequencies, and in HT cells we detected a small mode, which
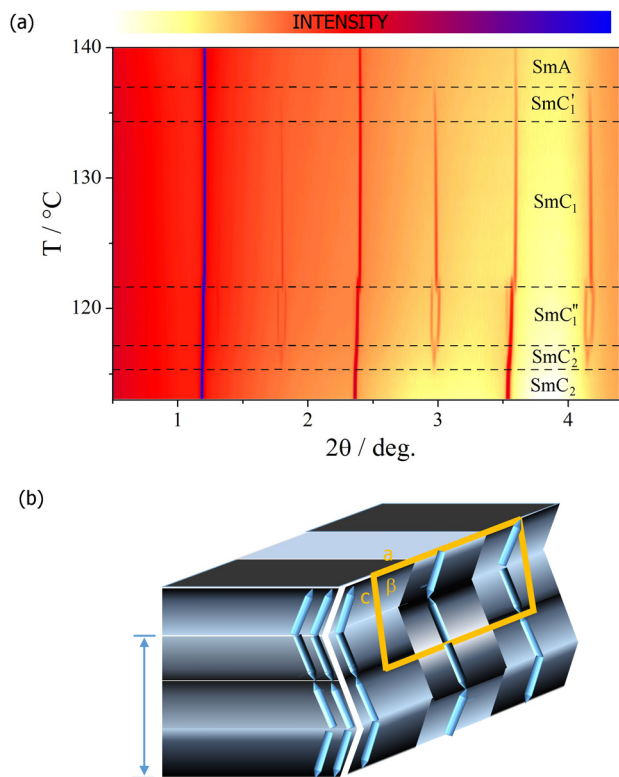
This journal is © The Royal Society of Chemistry 2024

J. Mater. Chem. C, 2024, **12**, 10903–10909 | **10907**

Fig. 8 (a) Temperature evolution of the small angle X-ray diffraction signals recorded for the **I-9** homologue in all the smectic phases. (b) Model of the modulated structure in which in-plane electron density modulations develop in the direction perpendicular to the tilt plane. The blue arrow shows a 3-layer basic periodicity related to the tilt arrangement, the yellow frame presents a 2D crystallographic unit, and parameter c corresponds to bilayer periodicity. Light/dark grey shadowing indicates the modulation of electron density due to the breaking of up/down symmetry of the molecules (schematically shown as blue pencils) within the layers.

can be attributed to a molecular rotation with respect to the molecular axis. For details, see ESI.† Fig. S7 shows 3-dimensional graphs of the imaginary part of permittivity for homologues **I-5** and **I-9**. Concerning the effect of an external electric field of up to 10 V μm^{-1}, no specific changes were detected in HG or HT cells under the field.

3. Conclusions

The most common tilted smectic phases exhibit either a synclinic (S) or anticlinic (A) arrangement of molecules within consecutive layers. In certain systems, the energy associated with these two packing modes is comparable, resulting in strong frustration that, for some rod-like molecules, might be relieved by building structures with a complex sequence of S and A interlayers. These structures might display a periodicity extending 3 up to several layers.[38] Conversely, the competition between the synclinic and anticlinic interactions may also be resolved by building structures with interfaces that are neither S nor A type. Moving from layer to layer, the molecules undergo rotation on the tilted cone at arbitrary angles between 0 and π,

leading to the formation of short helices, with clock (SmCα) or distorted clock-like structures: such structures for rod-like molecules are facilitated by molecular chirality.[1] Another scenario was found for bent dimers, where the interplay between the synclinic and anticlinic interactions leads to the formation of an incommensurate double helical structure,[14] in which an additional rotation of the molecular position on a tilted cone is superimposed on a short 4-layer helical unit cell.

Here, we investigated molecules with unique structures that have not yet been introduced. The presented rigid bent-core molecules have a bulky and polar end group attached through the flexible spacer. Depending on the length of the spacer, the phase behavior of the material drastically changes. The shorter homologues have a strong odd–even effect in the transition temperatures, which confirms that the bulky end group is either along the arm or inclined to the arm. For longer homologues, the conformational freedom of the spacer makes the transition temperatures less sensible to the spacer length. Nevertheless, for all short and long molecules, the competing anticlinic and synclinic interactions result in the formation of the extended multilayer periodic structures. In the case of short homologues, below the anticlinic SmC$_A$ phase, the bilayer structure adopts a helically modulated configuration (SmC$_{TB}$), optimizing energy by creating double interlocked helices with layer interfaces that are neither S nor A character, but exhibit a greater uniformity across the structure. In contrast, longer homologues accommodate competing interactions by establishing multilayer structures with a complex sequence of synclinic and anticlinic interfaces. As the temperature decreases, the ratio between the synclinic and anticlinic interfaces changes, yielding an 'apparent tilt' inversion. The specific structure relieving frustration depends on the strength of the interactions between the layers striving to maintain molecules within a single plane.

The molecular structure we introduced depends only on a borderline between calamitic, bent-shaped and dimeric structures. A really complicated interplay of structural aspects should be considered in the studied molecular system. Due to the observed stripe textures, such as those observed for twist-bend nematic and smectic phases,[8–14] we consider that the bent-shaped character of the molecular structure is partially suppressed. The prolonged shape and dimeric character of molecules produce the competing anticlinic and synclinic interactions of smectic mesophases. The present work contributes to the understanding of the complex character of fluid phase development, with a particular focus on the emergence of chiral structures from achiral molecules.

Data availability

The data set supporting this article has been included as part of the ESI.†

Conflicts of interest

The authors declare no conflict of interests.

10908 | *J. Mater. Chem. C*, 2024, **12**, 10903–10909

This journal is © The Royal Society of Chemistry 2024

Acknowledgements

References

1 *Handbook of Liquid Crystals*, ed. J. W. Goodby, P. J. Collings, T. Kato, C. Tschierske, H. F. Gleeson, P. Raynes, Wiley-VCH, Weinheim, 2014.

2 T. Niori, T. Sekine, J. Watanabe, T. Furukawa and H. Takezoe, *J. Mater. Chem.*, 1996, **6**, 1231.

3 D. R. Link, G. Natale, R. Shao, J. E. Maclennan, N. A. Clark, E. Korblova and D. M. Walba, *Science*, 1997, **278**, 1924.

4 H. Takezoe and Y. Takanishi, *Jpn. J. Appl. Phys.*, 2006, **45**, 597–625.

5 A. Jákli, *Liq. Cryst. Rev.*, 2013, **1**, 65.

6 H. Ocak, B. Bilgin-Eran, M. Prehm and C. Tschierske, *Soft Matter*, 2013, **9**, 4590.

7 L. E. Hough, M. Spanneth, M. Nakata, D. A. Coleman, C. D. Jones, D. Dantlgraber, C. Tschierske, J. Watanabe, E. Körblova, D. M. Walba, J. E. Maclennan, M. A. Glaser and N. A. Clark, *Science*, 2009, **325**, 452.

8 M. Cestari, S. Diez-Berart, D. A. Dunmur, A. Ferrarini, M. R. de la Fuente, D. J. B. Jackson, D. O. Lopez, G. R. Luckhurst, M. A. Perez-Jubindo, R. M. Richardson, J. Salud, B. A. Timimi and H. Zimmermann, *Phys. Rev. E*, 2011, **84**, 031704.

9 C. T. Imrie and P. A. Henderson, *Chem. Soc. Rev.*, 2007, **36**, 2096–2124.

10 J. P. Abberley, S. M. Jansze SM, R. Walker, D. A. Paterson, P. A. Henderson, A. T. M. Marcelis, J. M. D. Storey and C. T. Imrie, *Liq. Cryst.*, 2017, **44**, 68.

11 C. T. Imrie and G. R. Luckhurst. Liquid crystal dimers and oligomers. in *Handbook of Liquid Crystals*, ed. J. W. Goodby, P. J. Collings, T. Kato, C. Tschierske, H. F. Gleeson and P. Raynes, Wiley-VCH, Weinheim, 2014, vol. 4, pp. 137–210.

12 C. T. Imrie and G. R. Luckhurst. Liquid crystal dimers and oligomers. in *Handbook of Liquid Crystals*, ed. J. W. Goodby, P. J. Collings, T. Kato, C. Tschierske, H. F. Gleeson and P. Raynes, Wiley-VCH, Weinheim, 2014, vol. 7, pp. 137–210, and references cited therein.

13 R. J. Mandle, *Soft Matter*, 2016, **12**, 7883.

14 D. Pociecha, N. Vaupotic, M. Majewska, E. Cruickshank, R. Walker, J. M. D. Storey, C. T. Imrie, C. Wang and E. Gorecka, *Adv. Mater.*, 2021, **33**, 2103288.

15 M. G. Tamba, B. Kosata, K. Pelz, S. Diele, G. Pelzl, Z. Vakhovskaya, H. Kresse and W. Weissflog, *Soft Matter*, 2006, **2**, 60.

16 M. Horčic, J. Svoboda, A. Seidler, V. Kozmík, V. Novotná, D. Pociecha and E. Gorecka, *RSC Adv.*, 2016, **6**, 41972.

17 S. Umadevi, B. K. Sadashiva, H. N. Shreenivasa Murthy and V. A. Raghunathan, *Soft Matter*, 2006, **2**, 210.

18 G. Shanker, M. Prehm and C. Tschierske, *J. Mater. Chem.*, 2012, **22**, 168.

19 D. Kardas, M. Prehm, U. Baumeister, D. Pociecha, R. Amarantha Reddy, G. H. Mehl and C. Tschierske, *J. Mater. Chem.*, 2005, **15**, 1722.

20 M. Šepelj, A. Lesac, U. Baumeister, S. Diele, H. L. Nguyen and D. W. Bruce, *J. Mater. Chem.*, 2007, **17**(12 1154.

21 C. Tschierske, *Angew. Chem., Int. Ed.*, 2013, **52**, 8828.

22 B. K. Sadashiva, R. A. Reddy, R. Pratibha and N. V. Madhusudana, *J. Mater. Chem.*, 2002, **12**, 943.

23 E. Cruickshank, K. Anderson, J. M. D. Storey, C. T. Imrie, E. Gorecka, D. Pociecha, A. Makal and M. M. Majewska, *J. Mol. Liq.*, 2022, **346**, 118180.

24 V. Borshch, Y.-K. Kim, J. Xiang, M. Gao, A. Jakli, V. P. Panov, J. K. Vij, C. T. Imrie, M. G. Tamba, G. H. Mehl and O. D. Lavrentovich, *Nat. Commun.*, 2013, **4**, 2635.

25 G. Barbero, L. R. Evangelista, M. P. Rosseto, R. S. Zola and I. Lelidis, *Phys. Rev. E*, 2015, **92**, 032704.

26 S. J. Cowling, A. W. Hall and J. W. Goodby, *J. Mater. Chem.*, 2011, **21**, 9031.

27 J. P. Abberley, R. Killah, R. Walker, J. M. D. Storey, C. T. Imrie, M. Salamonczyk, C. Zhu, E. Gorecka and D. Pociecha, *Nat. Commun.*, 2018, **9**, 228.

28 K. Bajzíková, J. Svoboda, V. Novotná, D. Pociecha and E. Gorecka, *New J. Chem.*, 2017, **41**, 4672.

29 D. A. Coleman, J. Fernsler, N. Chattham, M. Nakata, Y. Takanishi, E. Körblova, D. R. Link, R.-F. Shao, W. G. Jang, J. E. Maclennan, O. Mondainn-Monval, C. Boyer, W. Weissflog, G. Pelzl, L.-C. Chien, J. Zasadzinski, J. Watanabe, D. M. Walba, H. Takezoe and N. A. Clark, *Science*, 2003, **301**, 1204–1211.

30 J. Svoboda, V. Novotná, V. Kozmík, M. Glogarová, W. Weissflog, S. Diele and G. Pelzl, *J. Mater. Chem.*, 2003, **13**, 2104.

31 V. Kozmík, M. Kuchař, J. Svoboda, V. Novotná, M. Glogarová, U. Baumeister and S. Diele, *Liq. Cryst.*, 2005, **32**, 1151.

32 A. Kovářová, V. Kozmík, J. Svoboda, V. Novotná, D. Pociecha and M. Glogarová, *Liq. Cryst.*, 2021, **39**, 755.

33 R. J. Mandle, S. J. Cowling and J. W. Goodby, *Phys. Chem. Chem. Phys.*, 2017, **19**, 11429–11435.

34 O. D. Lavrentovich, *Proc. Natl. Acad. Sci. U. S. A.*, 2020, **117**(26), 14629.

35 N. Podoliak, P. Salamon, L. Lejček, P. Kužel and V. Novotná, *Phys. Rev. Lett.*, 2023, **131**, 228101.

36 N. Vaupotič, M. Ali, P. W. Majewski, E. Gorecka and D. Pociecha, *ChemPhysChem*, 2018, **19**, 2566.

37 M. Ali, E. Gorecka, D. Pociecha and N. Vaupotič, *Phys. Rev. E*, 2020, **102**, 032704.

38 Y. Takanishi, I. Nishiyama, J. Yamamoto, Y. Ohtsuka and A. Iida, *Phys. Rev. E*, 2013, **87**, 050503(R).

This journal is © The Royal Society of Chemistry 2024

J. Mater. Chem. C, 2024, **12**, 10903–10909 | **10909**